Proceedings of the
International Conference on Mechanical Engineering 2007
(ICME2007) 29- 31 December 2007, Dhaka, Bangladesh

ICME07-FL-06

# EFFECT OF A DIAPHRAGM RUPTURE PROCESS ON FLOW CHARACTERISTICS IN A SHOCK TUBE USING DRIED CELLOPHANE

**Shigeru Matsuo[1], Mamun Mohammad[2], Shinya Nakano[3], Toshiaki Setoguchi[1] and Hey Dong Kim[4]**

[1] Dept. of Mechanical Engineering, Saga University, 1 Honjo-machi, Saga-shi, Saga 840-8502, Japan.
[2] Dept. of Mechanical Engineering, BUET, Dhaka-1000, Bangladesh.
[3] Graduate School of Science and Technology, Saga University, 1 Honjo-machi, Saga-shi, Saga 840-8502, Japan.
[4] School of Mechanical Engineering, Andong National University, 388, Songchun-dong, Andong 760749, Korea.

## ABSTRACT

Shock tubes are devices in which the state of a gas is changed suddenly from one uniform state to another by the passage of shock and expansion waves. In the theory of ideal shock tube flow, it is customarily assumed that the unsteady expansion and shock waves generated by diaphragm rupture are a perfectly centered plane wave. However, such waves are generally not centered, or may not even by plane in practice. In the present research, the numerical and experimental studies were carried out in order to investigate the effect of the diaphragm rupture process on the flow characteristics of expansion and shock waves generated near the diaphragm using dried cellophane.

**Keywords:** Compressible flow, Diaphragm Rupture, Shock Tube, Cellophane, Expansion Wave, Shock.

## 1. INTRODUCTION

For a shock tube with diaphragm, in order to simulate the flow induced simultaneously with diaphragm rupture accurately, it is important to estimate the process of diaphragm rupture. This becomes the important point of caution for investigation of formation distance of shock wave [1] and non-equilibrium condensation in the unsteady expansion wave [2].

In the flow in shock tube, there are some researches for the effect of rupture time of metal diaphragm and its opening time on shock Mach number [3-5]. From these researches, it is found that diaphragm rupture process is not instantaneous and the process is three-dimensional phenomenon which requires finite time. Furthermore, the opening time of diaphragm changes with initial pressure ratio, type of diaphragm, tube diameter and so on.

However, just it is shown qualitatively concerning effect of diaphragm rupture time. As far as we know, there are no researches investigating the process of diaphragm rupture quantitatively and precisely.

In the present research, the numerical study was carried out in order to investigate the effect of the diaphragm rupture process on the flow characteristics of expansion and shock waves generated near the diaphragm. The shock and expansion waves were generated by rapid bursting of a diaphragm sealing an expansion tube charged with dry air of atmospheric condition. In this study, the diaphragm of the shock tube was assumed to open in finite time and the opening rate of the diaphragm rupture was changed with time.

As a result, the effect of diaphragm rupture process on the flow field in the range close to the diaphragm was clarified, and the results obtained from numerical simulations were compared with the experimental ones using dried cellophane as a diaphragm.

## 2. CFD ANALYSIS

### 2.1 Governing Equations

The governing equations, i.e., the unsteady compressible Navier-Stokes equations written in an axisymmetric coordinate system $(x,y)$ are as follows :

$$\frac{\partial \boldsymbol{U}}{\partial t}+\frac{\partial \boldsymbol{E}}{\partial x}+\frac{\partial \boldsymbol{F}}{\partial y}=\frac{1}{Re}\left(\frac{\partial \boldsymbol{R}}{\partial x}+\frac{\partial \boldsymbol{S}}{\partial y}\right)+\frac{1}{y}\boldsymbol{H} \tag{1}$$

where

$$\boldsymbol{U}=\begin{bmatrix}\rho\\ \rho u\\ \rho v\\ E_t\end{bmatrix},\ \boldsymbol{E}=\begin{bmatrix}\rho u\\ \rho u^2+p\\ \rho uv\\ u(E_t+p)\end{bmatrix},\ \boldsymbol{F}=\begin{bmatrix}\rho v\\ \rho uv\\ \rho v^2+p\\ v(E_t+p)\end{bmatrix} \tag{2}$$

$$\boldsymbol{R}=\begin{bmatrix}0\\ \tau_{xx}\\ \tau_{xy}\\ \alpha\end{bmatrix},\ \boldsymbol{S}=\begin{bmatrix}0\\ \tau_{xy}\\ \tau_{yy}\\ \beta\end{bmatrix},\ \boldsymbol{H}=\begin{bmatrix}-\rho v\\ -\rho uv\\ -\rho v^2\\ -v(E_t+p)\end{bmatrix} \tag{3}$$

where

$$E_t=\rho C_{p4}T+\frac{1}{2}\rho\left(u^2+v^2\right) \tag{4}$$

$$p = (\gamma - 1)\left[ E_t - \frac{1}{2}\rho(u^2 + v^2) \right] \quad (5)$$

$$\alpha = u\tau_{xx} + v\tau_{yx} + \kappa \frac{\partial T}{\partial x},\ \beta = u\tau_{xy} + v\tau_{yy} + \kappa \frac{\partial T}{\partial y} \quad (6)$$

where $\boldsymbol{U}$ is the conservative vector, $\boldsymbol{E}$ and $\boldsymbol{F}$ are inviscid flux vector and $\boldsymbol{R}$ and $\boldsymbol{S}$ are viscous flux vectors. $\boldsymbol{H}$ is the source term corresponding to axisymmetry. $\tau_{xx}$, $\tau_{xy}$, $\tau_{yx}$ and $\tau_{yy}$ are components of viscous shear stress.

The governing equation systems that are non-dimensionalized with reference values at the atmospheric condition are mapped from the physical plane into a computational plane of a general transform. To close the governing equations, Baldwin-Lomax model [6] is employed in computations. A third-order TVD (Total Variation Diminishing) finite difference scheme with MUSCL [7] is used to discretize the spatial derivatives, and a second order-central difference scheme for the viscous terms, and a second-order fractional step is employed for time integration.

### 2.2 Computational Conditions

Computational domain of the shock tube for the present computational analysis is schematically shown in Fig.1. The number of grids is 1000×80. The shock tube has a length of 2000 mm. A diaphragm is located at the middle of the shock tube ($x$ = 0), and separates the high and low-pressure tubes. The shock tube has the diameter of $\phi D$ = 65.5 mm.

The pressures in the high and low-pressure tubes are defined as $p_4$ and $p_1$, respectively. In the present study, $p_4$ is kept constant at 101.3 kPa and the ratio of $p_4/p_1$ (= $p_{41}$) is changed from 2.0 to 4.0. In the present computations, $T_4$ (=$T_1$) is kept constant at 298.15 K.

Figure 2(a) and (b) show the straight diaphragm and the diaphragm with radius of circular arc, respectively. The ratio of radius of circular arc to the diameter of the shock tube $R_{dia.}/D$ was set in the range from 1.31 to 5.74.

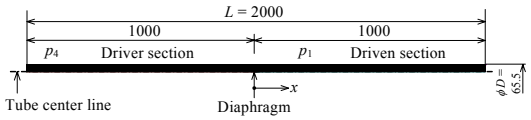


Fig 1: Computational domain (Unit : mm)

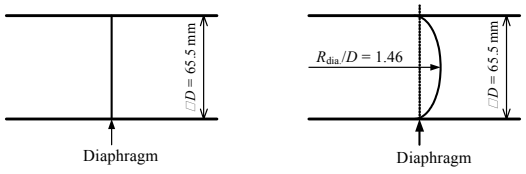


(a) Straight (b) Circular arc

Fig 2: Diaphragm

The radius $r$ of the diaphragm opening area at the arbitrary time $t$ is given by following equation.

$$t = \frac{\pi r^2}{\pi R^2} t_r = \left( (\frac{r}{R})^2 t_r \right) \quad (7)$$

where $t_r$ is the time of the diaphragm rupture which is obtained by experiment and $R$ (=$D$/2) is the radius of the shock tube.

Inlet and outlet boundaries are constrained to the free boundary conditions. Non-slip velocity and no heat transfer are constrained on the solid wall.

Figure 3 shows the process of diaphragm rupture in case of $t_r$ = 0.216 ($p_{41}$=2). Solid and dotted lines indicate the cases of opening corresponding to Eq.(7) (Type 1) and to Eq.(7) from $r/D$ =0.5 (Type 2). For Type 2, the diaphragm from $r/D$ =0 to 0.5 is spontaneous.

## 3. EXPERIMENTAL METHOD

A shock tube used in the present experiment has circular cross sectional area with diameter $\phi D$ = 65.5 mm. Figure 4 shows the details of shock tube. The driver and driven sections are separated by cellophane, and the diaphragm was ruptured by a needle. Initial conditions are the same as those of simulations. Pressure variations of the expansion wave propagating toward the driver section are measured by pressure transducers (PCB112A21) mounted at the positions of $x$ = -150 mm and -300 mm upstream of the diaphragm. Pressure signals were digitized with a time interval of 0.01 msec.

## 4. RESULTS AND DISCUSSION

Figure 5 shows relationships between and the initial pressure ratio $p_{41}$ and the time $t_r$ of diaphragm rupture obtained by experiment. As seen from this figure, the time decreases with an increase of the initial pressure ratio. For simulations, these times are used in order to investigate the flow field in the region close to the diaphragm.

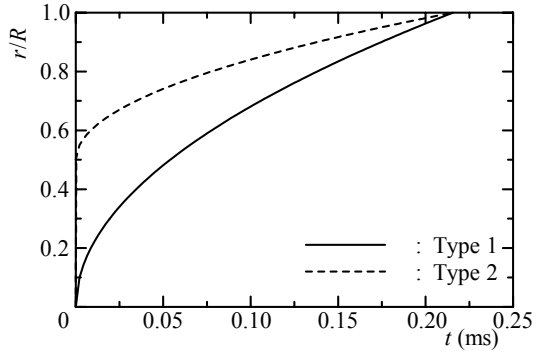


Fig 3: Diaphragm rupture speed ($p_4/p_1$ = 2.0)

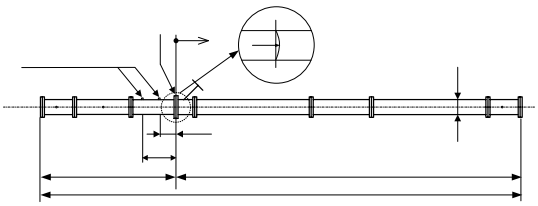

Fig 4: Test section (Unit : mm)

Figures 6(a) and (b) shows time histories of static pressure obtained from experiments and simulations in cases of straight diaphragm and diaphragm with radius of circular arc, respectively ($x/D$ = -2.29). The initial pressure ratio is $p_{41}$ = 2.0. The solid line in this figure shows experimental results. In this figure, the point that the pressure begins to decreases indicates the head of expansion wave, and the intersection point of each line with the line calculated by one-dimensional theory was considered as the tail of expansion wave. It is found that

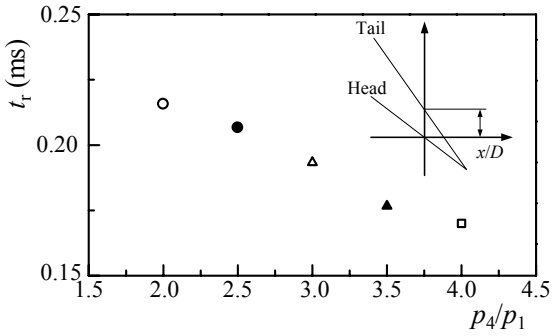


Fig 5: Relationships between the opening time of diaphragm and initial pressure ratio (Experiment)

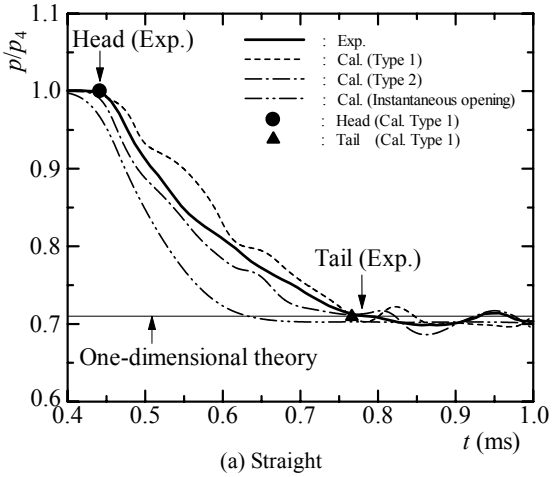


(a) Straight

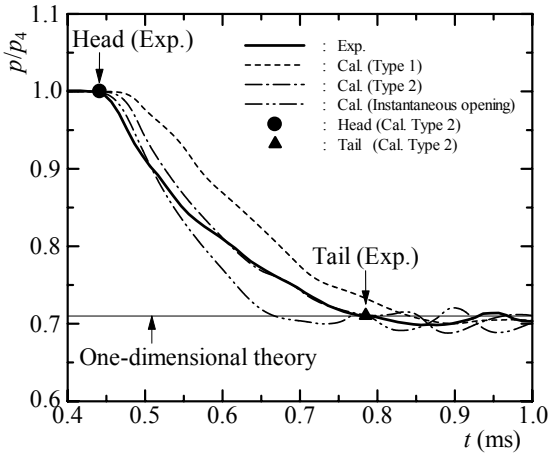


(b) Circular arc

Fig 6: Time histories of static pressure ($p_4/p_1$ = 2.0, $x/D$ =-2.29)

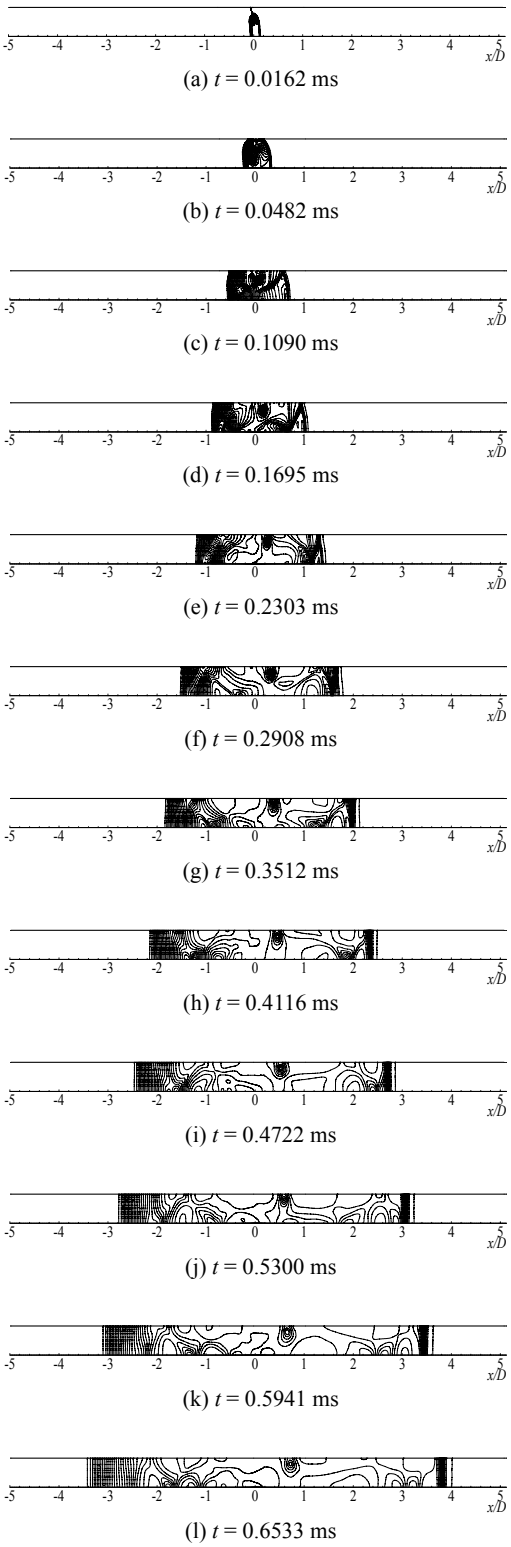


(a) $t$ = 0.0162 ms

(b) $t$ = 0.0482 ms

(c) $t$ = 0.1090 ms

(d) $t$ = 0.1695 ms

(e) $t$ = 0.2303 ms

(f) $t$ = 0.2908 ms

(g) $t$ = 0.3512 ms

(h) $t$ = 0.4116 ms

(i) $t$ = 0.4722 ms

(j) $t$ = 0.5300 ms

(k) $t$ = 0.5941 ms

(l) $t$ = 0.6533 ms

Fig 7: Contour maps of static pressure (Curve, Type 2, $p_4/p_1$ = 2.0)

simulated values agree well with experimental results. The reason of the static pressure variations in experiment and simulation after the tail reaches will be described

later.

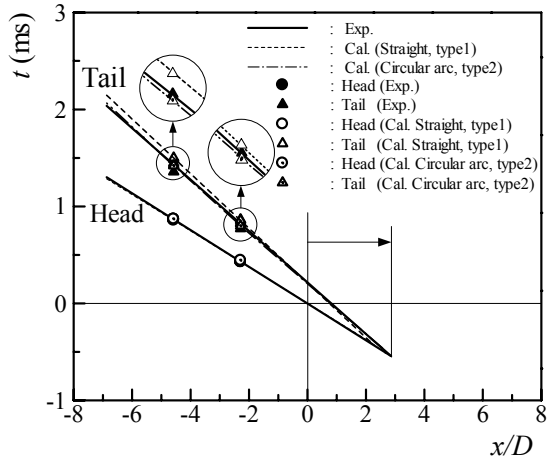


Fig 8: Wave diagram obtained by experiment and calculation ($p_4/p_1 = 2.0$)

Figure 7 is the contour maps of static pressure showing the process of the propagations of the shock wave and expansion wave in case of the diaphragm with radius of circular arc (Type 2). The initial pressure ratio is $p_4/p_1 = 2.0$. As seen from this figure, after the diaphragm rupture, the expansion and compression waves propagate in the driver and driven sections, respectively and the flow structure is highly two-dimensional. Furthermore, the expansion wave propagates with change of the strength continuously upstream of the diaphragm, and the spherical compression wave reflects at the wall of the tube as shown in Fig.7(c) and it propagates with change of the strength continuously in the same manner as the expansion wave. The flow near the diaphragm is not uniform and the complicated flow structure is confirmed even in Fig.7(l). It is considered from these figures that variations of the static pressure after the tail reaches as seen in Fig.6 is due to the complicated structure of these waves propagating in the tube.

Figure 8 shows wave diagrams obtained by experiment and calculation. The initial pressure ratio is $p_4/p_1 = 2.0$. The vertical and horizontal axes indicate the elapsed time from the diaphragm rupture and the distance along the tube axis, respectively. The open and close symbols are simulated and experimental results, respectively. The center position of the expansion wave is defined as the intersection point of each line of the head and tail of expansion wave. In one-dimensional theory, it is known that the center position of expansion wave is located at the origin. However, it is found in experiment that the center position of expansion wave is located at the position downstream of the origin.

Figure 9 shows the relationships between the initial pressure ratio $p_{41}$ and the distance $e$ from the origin to the center position of expansion wave as shown in Fig.8. The close and open symbols indicate experimental and simulated results, respectively. It is found that $e$ decreases with an increase of the initial pressure ratio and good agreement between experimental and simulated values is obtained.

Figure 10 shows the relationships between $p_{41}$ and the

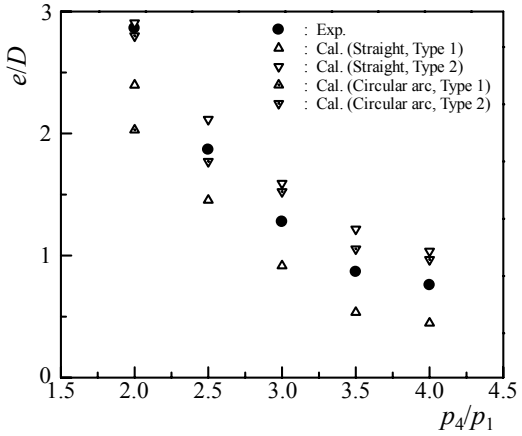


Fig 9: Relationships between initial pressure ratio $p_4/p_1$ and the distance of imaginary center $e$

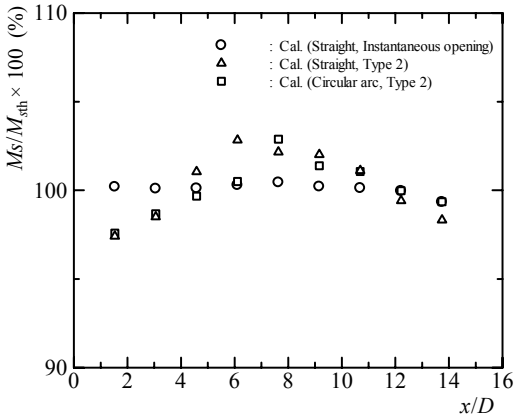


Fig 10: Relationships between shock Mack number $Ms$ and $x/D$ ($p_4/p_1 = 2.0$)

shock Mach number $M_s$. In this figure, $M_{sth}$ is the shock Mach number obtained by one-dimensional theory. As seen from this figure, the shock Mach number of Type 2 increases with an increase of $x/D$ and reaches maximum. After that, it decreases.

This variation showed similar tendency compared with experimental results obtained from the previous research [8]. Furthermore, the maximum of the shock Mach number and the corresponding distance from diaphragm agree nearly with the experimental results.

Judging from results of other cases, it is found that the rupture process of Type 2 with radius of circular arc reappears well the characteristics of flow obtained experimentally in case of the diaphragm using dried cellophane.

## 5. CONCLUSIONS

The numerical study was carried out in order to investigate the effect of the diaphragm rupture of the shock tube on the characteristics of expansion wave. As a result, it was found that the simulated values agreed well with experimental results, and the process of diaphragm rupture had a strong effect on variations of the static pressure in the shock tube.

## 6. REFERENCES


1. Ikui, T., et al., 1969, "Investigation of the Aerodynamics Characteristics of the Shock Tube (Part 2, On the Formation of Shock Waves)", Bulletin of JSME, vol.12, no.52, pp.783-792.
2. Matsuo, K., et al., 1982, "Relation between Condensation and Thermal Choking in an Unsteady Subsonic Flow, Bulletin of JSME, vol.25, no.203, pp.744-751.
3. Simpson, C.J.S.M., et al., Effect on Shock Trajectory of the Opening Time of Diaphragms in a Shock Tube, The Physics of Fluids, 10-9(1967), pp.1894-1896.
4. Rothkopf, E. M. and Low, W., Diaphragm opening process in shock tubes, The Physics of Fluids, 17-6(1964), pp.1169-1173.
5. White, D. R., Influence of diaphragm opening time on shock-tube flows, Journal of Fluid Mechanics, 4-6(1958), pp.585-599.
6. Baldwin B.S., Lomax, H., 1978, "Thin layer approximation and algebraic model for separated turbulent flows", AIAA Paper, No. 78(257).
7. Yee, H.C., 1989, "A class of high-resolution explicit and implicit shock capturing methods", NASA TM-89464.
8. Ikui, T., et al., 1969, "Investigation of the Aerodynamics Characteristics of the Shock Tube (Part 1, The Effects of Tube Diameter on the Tube Performance)", Bulletin of JSME, vol.12, no.52, pp.774-782.


## 7. NOMENCLATURE

| Symbol | Meaning | Unit |
|---|---|---|
| $C_p$ | Specific heat at constant pressure | (J/kg·K) |
| $D$ | Diameter of the shock tube | (m) |
| $e$ | Distance of center positon of expansion wave | (-) |
| $\boldsymbol{E}$, $\boldsymbol{F}$ | Inviscid flux vectors | (-) |
| $E_t$ | Total energy per unit volume | ($J/m^3$) |
| $\boldsymbol{H}$ | Source term for axsimmetry | (-) |
| $L$ | Tube length | (-) |
| $M_s$ | Shock Mach number | (-) |
| $M_{sth}$ | Shock Mach number obtaind by one-dimensional theory | (-) |
| $p$ | Pressure | (Pa) |
| $R$ | Radius of the tube | (m) |
| $R_{dia}$ | Radius of circular ace | (m) |
| $\boldsymbol{R}$, $\boldsymbol{S}$ | Viscous flux vectors | (-) |
| $Re$ | Reynolds number | (m) |
| $r$ | Diameter of opening area of diaphragm | (m) |
| $T$ | Temperature | (K) |
| $t$ | Time | (s) |
| $t_r$ | Time of the diaphragm rupture | (s) |
| $\boldsymbol{U}$ | Conservative vector | (-) |
| $u$, $v$ | Velocity components | (m/s) |
| $x$, $y$ | Cartesian coordinates | (m) |
| Greeks | | |
| $\gamma$ | Ratio of specific heats | (-) |
| $\kappa$ | Thermal conductivity | (W/m·K) |
| $\rho$ | Density | ($kg/m^3$) |
| $\tau$ | Shear stress | (Pa) |
| Subscripts | | |
| 1 | Initial state of driven section | |
| 4 | Initial state of driver section | |